Random Phase Approximation/Semiempirical Computations of Electronic Structure of Extended Organic Molecules

Sergei Tretiak
Theoretical Division,
Los Alamos National Laboratory,
Los Alamos, New Mexico 87545
serg@lanl.gov

(July 31, 2001)
Submitted to "Recent Research Developments in Physical Chemistry", 5th issue (India)
Reference No: TRN/CP/E-59

ABSTRACT

This article reviews recent studies of excited states and optical properties of organic molecular systems based on the Random Phase Approximation combined with INDO/S, MNDO, AM1, and PM3 semiempirical Hamiltonian models. Fast Krylov-space based algorithms for the required diagonalization of large Hamiltonian matrices make possible to calculate excited state structure of organic molecular systems with hundreds of heavy atoms with only moderate computational effort. This technique is applied to compute the electronic structure of large conjugated molecules and molecular aggregates. To mimic the experimental conditions, the solvent contributions are incorporated using the Self-Consistent Reaction Field approach. Calculated spectroscopic observables (excited-state energies, oscillator strengths and polarizabilities) agree well with experimental data and each other. In particular, the results obtained with the Hamiltonians parameterized for ground-state calculations such as AM1 and PM3 agree well with the INDO/S results. Subsequent two-dimensional real-space analysis of corresponding transition density matrices provides an efficient way for tracing the origin of various optical transitions by identifying the underlying changes in charge densities and bond-orders.

I. INTRODUCTION

Technologies based on organic materials for opto-electronic devices today have become a reality and in the near future may well compete with semiconductor and liquid crystal based traditional approaches. Potential technological applications include electroluminescent [1–3], photovoltaic [4], and optoelectronic [5–7] devices, photodetectors [8,9], transistors [10,11], solid state lasers [12–17], optical limiting materials [18]. One of the key points in the development of such technologies is the synthesis of molecular structures with desired functionalities.

Accurate calculations of molecular vertical excitation energies and polarizabilities are essential for the modeling of spectroscopic probes, addressing structure-function relations and predicting structures with desired optical properties [19–21]. Generating a qualitatively acceptable description of excited states is a much more challenging task than analogous ground state calculations. The reason is that the ground state electronic wavefunction is usually well approximated by a single Slater determinant, whereas much more complicated configuration interaction (CI) representations are often needed for the excited states [22]. The large computational demand associated with CI calculations places severe limitations on the size of the systems whose excited states can be studied [23]. Alternatives to CI approaches such as time-dependent density functional theory (DFT) [24–26] are now available within the standard quantum chemistry packages (e.g. Gaussian [27]). While we are still accumulating experience with these techniques, it appears that they produce quite reasonable spectra, especially when used with the new generation of gradient-corrected or hybrid functionals. However, while applicable to larger systems than traditional CI calculations, they are still fairly computationally expensive. To our knowledge, the largest system studied with these techniques to date is the C_{70} cluster [24].

Calculation of nonlinear molecular polarizabilities is a closely related task. The Coupled-Perturbed Hartree-Fock (CPHF) approach computes polarizabilities by evaluating energy derivatives of a molecular Hamiltonian perturbed by an external field [19]. Usually combined with semiempirical or *ab initio* Hamiltonians, this method involves substantial computational effort especially in the latter case. A second method uses time-dependent perturbation theory, which relates optical response to the properties of the excited states. The Configuration-Interaction/Sum-over-States (CI/SOS) [19–21,28] approach involves the calculations of both the ground state and excited state wavefunctions and the transition dipole moments between them. This method is not necessarily size-consistent (intrinsic interference effects resulting in near cancellation of very large contributions further limit its accuracy) and special care needs to be taken when choosing the right configurations. On the other hand, the experimental measurements are usually conducted in condensed phase, and therefore all spectroscopic observables are heavily influenced by intermolecular coupling in solid state or solute-solvent interactions in solution which makes comparison of calculations with experiment very tedious.

In this review we focus on RPA techniques used in conjunction with the semiempirical approaches developed to target larger system sizes [29–33]. These approaches are based on simplified Hamiltonians parameterized using high-level *ab initio* calculations and (or) experimental data. The semiempirical approximations usually limit the basis set to a minimum valence basis of Slater type orbitals. Coulomb and exchange terms in the two-electron interaction are approximated and many are ignored completely. Typically, only one- and two- center Coulomb interactions are retained, and the exchange interactions are usually limited to those on a single atom. These approximations make semiempirical techniques fast and efficient yet reasonably accurate for computation of molecular properties. In particular the recently developed Collective Electronic Oscillator (CEO) approach [34,35] is based on the time-dependent Hartree-Fock (TDHF) approximation or Random Phase Approximation (RPA) [36,37] for many-electron wavefunction and used the ground state density matrix and semiempirical Hamiltonian as an input. This method provides a powerful tool for studying the optical response of large conjugated and aggregated molecules [34,35,38] and has been successfully used in calculations of the optical properties of a variety of conjugated chromophores such as porphyrins, dendrimers, donor/acceptor polymers, biological light-harvesting complexes, etc. [34,39,40]. By focusing only on the spectroscopically relevant observables, the CEO enables calculations on excited electronic states of molecules with hundreds of heavy atoms. In this article we review some recent results obtained with the CEO approach for photoluminescent polymers and donor/acceptor substituted conjugated molecules.

Section II describes the computational method. In Section III we analyze the electronic spectra of conjugated oligomers and their aggregates and nonlinear optical polarizabilities of donor/acceptor substituted molecules computed with different semiempirical techniques. Finally, we summarize the results in Section IV.

II. THE RPA/SEMIEMPIRICAL FORMALISM

The numerical CEO method for computing electronic structure is described in detail elsewhere [34,35,41]. The procedure starts with molecular geometry, optimized using standard quantum chemical methods [27], or obtained from experimental X-ray diffraction or NMR data. INDO/S, AM1, PM3, MNDO, and MINDO/3 semiempirical Hamiltonians (Section II A) are then generated for each optimal molecular structure using either ZINDO (INDO/S) [42,43] or the MOPAC-93 (AM1, PM3, MNDO, and MINDO/3) code [44]. The Hartree-Fock ground state density matrix is calculated next. These density matrix and hamiltonian are the input into CEO calculations which solve the TDHF equation of motion by the diagonalization of the Liouville operator (Section II B). The latter could be efficiently performed using Krylov-space techniques: IDSMA [34,35,45], Lanczos [41,46,47], or Davidson's [48,24] algorithms. Two-dimensional representation of the resulting transition density matrices provides an analysis of each electronic transition and molecular optical response in terms of excited state charge distribution and motions of electrons and holes in real space (Section III). Finally, computed vertical excitation energies and transition densities may further be used to calculate molecular spectroscopic observables such as transition dipoles, oscillator strengths, linear absorption, and static and frequency-dependent nonlinear responses (Sections II B and III). The overall scaling of these computations does not exceed K^3 in time and K^2 in memory (K being the basis set size) for both ground and excited state (per state) calculations. Typically, direct diagonalization of the Liouville operator L or CI Singles matrix A without invoking Krylov-space methods decreases the computational efficiency to $\sim K^6$ in time and $\sim K^4$ in memory for the excited states.

A. Molecular Hamiltonian and semiempirical approximation

Let us consider a general system of N electrons which can occupy K single-electron states ($N \leq K$) and interact with an external field. The Hamiltonian in second quantization form is most generally given by [22]

$$\widehat{H} = \sum_{mn\sigma} t_{mn} c^\dagger_{m\sigma} c_{n\sigma} + \sum_{\substack{mnkl \\ \sigma\sigma'}} \langle nm|kl\rangle c^\dagger_{m\sigma} c^\dagger_{n\sigma'} c_{k\sigma'} c_{l\sigma} - \sum_{mn\sigma} \boldsymbol{\mathcal{E}}(t) \cdot \boldsymbol{\mu}_{mn} c^\dagger_{m\sigma} c_{n\sigma}, \tag{2.1}$$

where the subscripts i, j, k, l run over known spatial atomic basis functions $\{\chi_n\}$ and σ, σ' label spin components. These atomic orbitals are assumed to be orthogonal and $c^\dagger_n (c_n)$ are the creation (annihilation) operators which satisfy the Fermi anticommutation relations

$$c_{m\sigma} c^\dagger_{n\sigma'} + c^\dagger_{n\sigma'} c_{m\sigma} = \delta_{mn} \delta_{\sigma\sigma'}, \tag{2.2}$$

and all other anticommutators of $c^\dagger$ and c vanish.

For clarity, we hereafter focus on closed-shell molecules and exclude spin variables assuming that N electron pairs occupy K spatial atomic orbitals. Generalization to the unrestricted opened-shell case and non-orthogonal basis set is possible [22]. The first term in Eq. (2.1) is the core-hamiltonian describing the kinetic energy and nuclear attraction of an electron

$$t_{nm} = \langle n| - \frac{1}{2}\nabla_1^2 - \sum_A \frac{Z_A}{|\mathbf{r}_1 - \mathbf{R}_A|} |m\rangle \equiv \int d\mathbf{r}_1 \chi^*_n(1) \left(-\frac{1}{2}\nabla_1^2 - \sum_A \frac{Z_A}{|\mathbf{r}_1 - \mathbf{R}_A|} \right) \chi_m(1), \tag{2.3}$$

where $\mathbf{R}_A$ is the nuclear coordinate of atom A. The second term represents electron-electron Coulomb interactions where

$$\langle nm|kl\rangle = \int d\mathbf{r}_1 d\mathbf{r}_2 \chi^*_n(1) \chi^*_m(2) \frac{1}{r_{12}} \chi_k(1) \chi_l(2), \tag{2.4}$$

are the two-electron integrals. The interaction between the electrons and the external electric field $\boldsymbol{\mathcal{E}}(t)$ is given by the last term in Eq. (2.1), $\boldsymbol{\mu}$ being the dipole operator

$$\boldsymbol{\mu}_{nm} = \langle n|\boldsymbol{\mu}|m\rangle \equiv \int d\mathbf{r}_1 \chi_n^*(1)\mathbf{r}_1\chi_m(1). \quad (2.5)$$

To solve the Schrödinger equation $\widehat{H}\Psi = E\Psi$ for the ground state we assume the simplest antisymmetric wavefunction i.e a single Slater determinant $\Psi = |\phi_1(1)\phi_2(2)\ldots\phi_N(N)>$ [22] (Hartree-Fock approximation). Here $\{\phi_\alpha\}$ are the molecular orbitals (MO). Following Roothaan's procedure [22] they are expanded as linear combinations of spatial atomic basis functions $\{\chi_n\}$

$$\phi_\alpha = \sum_i^K C_{\alpha i}\chi_i. \quad (2.6)$$

The Hartree-Fock approximation replaces the complex many-body problem by an effective one-electron problem in which electron-electron repulsion is treated in an average (mean field) way. The Hartree-Fock eigenvalue equation is derived by minimizing the ground state energy with respect to the choice of MOs

$$FC = C\epsilon. \quad (2.7)$$

This equation may be recast in the form

$$[F(\bar{\rho}), \bar{\rho}] = 0. \quad (2.8)$$

The ground-state density matrix $\bar{\rho}$ is related to the MO expansion coefficients (Eq. (2.6)) for closed-shells as

$$\bar{\rho}_{nm} = \sum_a^{N_{occ}} C_{na}C_{ma}^* = 2\sum_a^N C_{na}C_{ma}^*. \quad (2.9)$$

$F(\bar{\rho})$ is the Fock matrix with matrix elements

$$F_{nm}(\bar{\rho}) = t_{nm} + V_{nm}(\bar{\rho}), \quad (2.10)$$

and the matrix representation of the Coulomb electronic operator V in the atomic basis set $\{\chi_n\}$ is

$$V(\bar{\rho})_{mn} = \sum_{k,l}^K \bar{\rho}_{kl}[\langle mk|nl\rangle - \frac{1}{2}\langle mn|kl\rangle]. \quad (2.11)$$

The Hartree-Fock equation (2.7) is nonlinear and may be readily solved iteratively using the self consistent field (SCF) procedure [22].

In all computations presented below we use semiempirical parameterizations of the hamiltonian (2.1). This approximation limits the basis set to a minimum valence basis of Slater type orbitals. Coulomb and exchange terms in the two-electron interaction are approximated and many are ignored completely. Typically, only one- and two- center Coulomb interactions are retained, and the exchange interactions are usually limited to those on a single atom:

$$\langle\chi_n^A\chi_k^B|\chi_m^A\chi_l^B\rangle = \begin{cases} \langle\chi_n^A\chi_k^A|\chi_m^A\chi_l^A\rangle & A = B \\ \langle\chi_n^A\chi_k^B|\chi_n^A\chi_k^B\rangle\delta_{nm}\delta_{kl} & A \neq B \end{cases} \quad (2.12)$$

where χ_n^A belongs to atom A and χ_n^B to atom B. The tetradic matrix $\langle\chi_n\chi_k|\chi_m\chi_l\rangle$ thus becomes block-diagonal in two dimensions. Thus this approximation allows to limit the number and store all computed Coulomb matrix elements in memory instead of recalculating them when needed as is commonly done in *ab initio* computations, making semiempirical techniques significantly easier and faster.

The semiempirical Hamiltonians which have evolved over the years differ both in the types of two-electron integrals retained in the model, and the manner in which the relevant parameters are determined. In particular, to study excited states, M. C. Zerner [42,43] combined the Intermediate Neglect of Differential Overlap (INDO) model of Pople and coworkers [29] with a CI method to generate excited states. The CI expansion was limited to single excitations from the ground state determinant, an approach dubbed the CI singles (CIS) approximation. The original INDO parameters did not work well, but Zerner found that the model could be reparameterized to reproduce the vertical excitation energies of small organic molecules and transition metal compounds [42,43]. This method was christened the INDO/S [INDO/spectroscopy] approach and has proven to be an extremely valuable technique [49]. INDO/CIS calculations have been successfully applied to studies of electronically excited states in a wide variety of chromophores, including transition metals [42,50,51]. The ZINDO code developed by Zerner and coworkers serves as a convenient platform for these calculations. We found that the RPA combined with the INDO/S Hamiltonian works extremely well without further reparameterization for many molecules and thus provides an alternative approach for computing the optical properties of a broad range of molecules [34,35,38–40]. However, reproducing the excitation energies came at a price, however, as the INDO/S method does very poorly for ground state geometries. In applications, typically either the experimental geometry or a semiempirical approach developed for the ground state is used to determine the geometry of the molecule, and is followed by an INDO/S calculation to generate the excited states.

The other family of semiempirical models developed by Dewar and Stewart [30–33] adjusted their parameters to reproduce the ground state geometry, heats of formation and other properties at Hartree-Fock level. This approach assumes that electron correlation effects can be incorporated in the empirically determined parameters. The models of choice for the ground state [Austin Model 1 (AM1) [30], Parametric Model 3 (PM3) [31], Modified Intermediate Neglect of Diatomic Overlap (MNDO) [32] and older Modified Intermediate Neglect of Differential Overlap 3 (MINDO/3) [33]] are the basis for MOPAC 2000 package which is a convenient and very fast platform for studying chemical properties and reactions in gas. The accuracy of these semiempirical approaches in prediction of numerous chemical and physical properties such as Gibbs free energies, activation energies, reaction paths and dipole moments, rivals that of much more numerically demanding *ab initio* and Density Functional Theory (DFT) methods.

However these models have not been systematically studied as regards their applicability to excited states, presumably because of the success of INDO/S and the availability of the ZINDO molecular orbital package [49]. Recently, the applicability of the CEO techniques combined with semiempirical Hamiltonians other than INDO/S has been examined. The motivation is that we would like to treat both the ground state and its excitations within the same model Hamiltonian. As was mentioned earlier, the INDO/S parameterization does not work well for ground state properties such as the equilibrium geometry. An example where a unified treatment would be particularly useful is in the generation of excited state potential energy surfaces by adding an excitation energy to a ground state energy [52–54]. This is particularly awkward if one Hamiltonian must be used to generate the ground state surface and another to determine the excitation energy. In this review we also compare the results of the CEO/AM1 and CEO/PM3 combinations with the CEO/INDO/S model and also with experiment.

In order to include the effects of the surrounding medium it is possible to use the Self-Consistent Reaction Field (SCRF) approach [55–58], in which the interaction energy between a solute and the surrounding medium is added to the HF energy of an isolated molecule, and the total energy of the system is then minimized self-consistently. In the electrically neutral solute, only the dipolar interactions contribute to the solvation energy. Assuming that the solute is separated from the solvent by a sphere of radius a_o the expression for this Onsager dipolar term has been derived in [56,57]. The Fock operator F^0_{mn} [22] is then modified by adding the response of a dielectric medium, resulting in:

$$F_{mn} = F^0_{mn} - \frac{\epsilon - 1}{2\epsilon + 1} \frac{\boldsymbol{\mu}_g \cdot \boldsymbol{\mu}_{mn}}{a_o^3}, \qquad (2.13)$$

where F^0_{mn} is the isolated complex Fock operator, ϵ is the dielectric constant, and a_o is a cavity radius. $\boldsymbol{\mu}_g$ is the ground-state dipole moment given by the expectation value of the molecular dipole operator $\boldsymbol{\mu}$. A reasonable estimate for the radius of the Onsager solvent reaction field model (a_o) is readily available in the standard Gaussian 98 package [27]. Onsager's SCRF is the simplest method for taking dielectric medium effects into account and more accurate approaches have been developed [59,60]. Here, an effective sphere model captures the essential solvent effect and is a reasonable approach within semiempirical approximations. For example, this CEO/SCRF approach has been successfully applied to compute electronic excitations in biological light-harvesting complexes which are significantly affected by protein environment effects [62]. Although the shape of the cavity has some effect on the molecular electronic structure [61], the methods taking into account "real" molecular shapes are computationally expensive and are most appropriately utilized with accurate *ab initio* or DFT approaches [61].

B. The RPA eigenvalue problem.

The CEO procedure computes the excited states using each set of semiempirical Hamiltonian parameters, Onsager dipolar terms, and HF ground state density matrices. This method, described in detail elsewhere [34,35][1], solves equations of motion for the reduced single-electron density matrix [63,64] given by

$$\rho_{mn} = \langle \Psi(t) | c_m^\dagger c_n | \Psi(t) \rangle, \tag{2.14}$$

where $\Psi(t)$ is the many-electron wavefunction.

When the molecule is driven by an external field, its density matrix acquires a time-dependent part. In the frequency domain, we decompose the density matrix into a ground state contribution $\bar{\rho}$ and a field-induced part

$$\begin{aligned}\rho_{mn}(\omega) = \bar{\rho}_{mn} + \delta\rho^{(1)}_{mn}(\omega) \\ + \delta\rho^{(2)}_{mn}(\omega) + \delta\rho^{(3)}_{mn}(\omega) + \cdots,\end{aligned} \tag{2.15}$$

where $\delta\rho^{(k)}_{mn}(\omega)$ is the kth order contribution from the incoming optical field. The diagonal elements $\delta\rho^{(k)}_{mm}$ represent the charge densities induced at the mth AO by the external field, whereas the off-diagonal elements $\delta\rho^{(k)}_{mn}$ with $m \neq n$ reflect the optically induced coherence between the mth and nth AO, which represents the probability of finding an electron-hole pair with the electron (hole) located at the mth (nth) AO. The density matrix thus provides a real-space picture of the optical response order by order in the driving field, as explored in detail in [34,39]. The polarization can be then expressed in terms of the density matrix as

$$P^{(k)} = \sum_{nm} \mu_{nm} \delta\rho^k_{mn}. \tag{2.16}$$

The polarizabilities α, β and γ are related to $P^{(1)}$, $P^{(2)}$ and $P^{(3)}$, respectively. The linear polarizability, for example, is given by

$$\alpha(\omega) = \sum_\nu \frac{2\Omega_\nu \mu_{g\nu} \mu^*_{g\nu}}{\Omega^2_\nu - (\omega + i\Gamma)^2}, \tag{2.17}$$

where Γ is a dephasing rate, $\mu_\nu = Tr(\mu\xi_\nu)$ is the transition dipole moment for νth electronic state, and Ω_ν are the transition frequencies. In an analogous way, the second (β) and the third (γ) order off-resonant nonlinear polarizabilities can be expressed in terms of frequencies and transition dipole moments [34,35,37].

The CEO calculates $\delta\rho^{(k)}_{mn}(\omega)$ by expanding it into a superposition of transition density matrices (denoted the *electronic normal modes*, ξ_ν), representing the electronic transition between the ground state $|g\rangle$ and an electronically excited state $|\nu\rangle$, given by

$$(\xi_\nu)_{mn} = \langle g | c_m^\dagger c_n | \nu \rangle. \tag{2.18}$$

[1] In practice, computation in the dielectric medium is conducted by replacing the isolated complex Fock operator F^0_{mn} by a Fock operator in the dielectric medium F_{mn} according to the procedure outlined in [34,35].

The electronic modes are computed as eigenmodes of the linearized TDHF equations of motion for the density matrix[2]. The eigenfrequencies Ω_ν of these equations provide the optical transition energies [34,37,65,66]:

$$L\xi_\nu = \Omega_\nu \xi_\nu \qquad L\xi_\nu^\dagger = -\Omega_\nu \xi_\nu^\dagger$$
$$\nu = 1, \ldots, K^2/2. \tag{2.19}$$

L is a linear operator in Liouville space (i.e. superoperator) with transition densities ξ_ν being its eigenvectors [34,35]. In the restricted TDHF scheme [37] only particle-hole and hole-particle components of ξ_ν are computed. Therefore, this non-hermitian eigenvalue problem of dimension $2M \times 2M$, $M = N_{occ} \times N_{vir} = N \times (K - N)$ in MO basis set representation is given by

$$\begin{pmatrix} A & B \\ -B & -A \end{pmatrix} \begin{bmatrix} X \\ Y \end{bmatrix} = \Omega \begin{bmatrix} X \\ Y \end{bmatrix}. \tag{2.20}$$

This is known as the RPA eigenvalue equation [67,24], where X and Y are, respectively, the particle-hole and hole-particle components of the transition density $\xi = \left[\begin{smallmatrix} X \\ Y \end{smallmatrix}\right]$ in MO representation [24,37,67,68]. In Eq. (2.20) the matrix A is hermitian and identical to the CI Singles matrix, whereas the hermitian matrix B represents higher order electronic correlations which are included in the TDHF approximation.

Direct diagonalization of the TDHF operator L or the CIS operator A in Eq. (2.20) is the bottleneck, requiring computational effort which scales as $\sim K^6$ in time and $\sim K^4$ in memory (for comparison, SCF ground state calculations scales as $\sim K^3$ in time and $\sim K^2$ in memory) because we are working in the space of higher dimensionality (electron-hole pairs). Direct diagonalization of Eq. (2.20) results in all excited states which span the entire spectral region. The traditional quantum-chemical approach addresses this problem by limiting the total basis set size variables K to a few MOs which are "important" for visible-uv optical response. Indeed most of the electronic states obtained by diagonalization of Eq. (2.20) lie in the X-ray spectral region and correspond to atomic-core type transitions. Visible-uv collective molecular excitations on the other hand could be well described by taking into account only few MOs close to HOMO-LUMO energy gap by truncating an active space. Although this approach works quite well and the ZINDO code [42,50,51] became very successful, truncating the active space is a complicated and to some extend arbitrary procedure. In addition, even truncated CI calculations are usually significantly more expensive than ground state computations.

An alternative solution to this problem is provided by fast Krylov-space algorithms [69,70]. These algorithms construct a small subspace of orthogonal vectors which contains a good approximation to the true eigenvector. This Krylov subspace $Sp\{\xi, L\xi, L^2\xi, \ldots, L^j\xi\}, j \ll M$, spans the sequence of vectors generated by the power method (the multiple action of the RPA operator L on the initial vector ξ). These methods find several eigenvalues and eigenvectors of large matrix L using only matrix-vector operations [69,70]. Indeed, usually only a small fraction of eigenstates of L (~ 100) lie in the visible-uv region and are of interest for optical spectroscopy. In addition, the action of the TDHF operator L on an arbitrary matrix ξ which contain particle-hole and hole-particle components is given by

$$L\xi = [F(\bar{\rho}), \xi] + [V(\xi), \bar{\rho}], \tag{2.21}$$

This product may therefore be constructed directly and the full matrix L is never stored in memory [37,35,34]. The action of the CIS operator A on an arbitrary matrix ξ can be also computed directly [48,71] (e.g. using Eq. (2.21) by setting the hole-particle component of ξ to zero). Eq. (2.21) holds in an arbitrary representation (e.g. site). The cost of such operation in

[2]The TDHF coincides with the Random Phase Approximation (RPA) for the linear optical response of many-electron systems (e.g. Chapter 8.5 in [36]). The electronic modes are identical to the transition densities of the RPA eigenvalue equation.

Hilbert $K \times K$ space scales as $\sim K^3$ in time and $\sim K^2$ in memory with system size. Computing a single eigenvalue-eigenvector of matrix L which corresponds to molecular excited state thus requires a computational effort comparable to that of the ground state.

There are several types of Krylov-space based algorithms. The original Lanczos algorithm computes effectively the lowest eigenvalue and the corresponding eigenvector of a large Hermitian matrix [69]. Since the matrices L that need to be diagonalized in the TDHF or adiabatic TDDFT approaches are non-Hermitian, the standard Lanczos algorithm is not applicable, and the modified Lanczos algorithm should be used instead [41,46,46]. Similarly, Davidson's algorithm originally formulated for the diagonalization of large Hermitian CI matrices [48] was further modified for the TDHF [67,72] and adiabatic TDDFT [24,68] methods. A third method for computing the lowest frequency eigenmode of a large Hamiltonian matrix is based on the Iterative Density Matrix Spectral Moments Algorithm (IDSMA) [34,35]. All three algorithms show similar scaling of computational time, resulting from $K \times K$ matrix multiplications. However, the scaling prefactors are different. The Davidson type algorithms, especially the recently improved versions [24,68], are extremely fast but I/O (input/ouput) intensive, since one needs to keep all the previous iterations for the eigenmodes throughout the iteration procedure. This fast convergence is ensured by Davidson's preconditioning, which assumes that the matrices L (or A) are dominated by their diagonal elements [48]. The Lanczos method usually requires larger Krylov-space dimension to obtain an approximate eigenvalue with the same accuracy as Davidson's algorithm, however, it needs to keep only 3 expansion vectors. Orthogonality among expansion vectors is automatically ensured by Lanczos recursion relations [69,41]. Even though the IDSMA is slower than the Lanczos, it has low memory requirements and allows to compute both "exact" eigenstates and "effective" eigenstates. The latter may represent overall contribution from several electronic states into optical response by a single effective state [34,35]. This provides an approximation for the spectrum in terms of very few variables [39]. None of these three algorithms is universally superior and the method of choice depends on the specific application.

Since all algorithms converge to the lowest eigenmode, the higher eigenmodes can be successively obtained by finding the lowest mode in the subspace orthogonal to that spanned by the lower modes already found [69]. This orthogonalization procedure is not always stable, leading to the accumulation of numerical error for the higher frequency modes. Alternatively a deflection procedure [69,41] that involves the antisymmetric "scalar product" (known as the symplectic structure) [37] may be used to avoid this problem.

III. APPLICATIONS

In this Section we illustrate the CEO approach analyzing electronic structure and optical properties of linear polymers [35,39,45] and donor/acceptor substituted oligomers [73–75]. The CEO has been applied to other molecular systems such as chlorophylls [58,76,77], naphthalene [78] and PPV dimers [40,79,80], phenylacetylene dendrimers [38,81] and photosynthetic light-harvesting antenna complexes [58,62] as well.

A. Electronic excitations of conjugated oligomers and their aggregates.

Conjugated oligomers of polyacetylene (PA), polydiacetylene (PDA), polytriacetylene (PTA), poly-phenylenevinylene (PPV), poly-*p*-phenylene (PPP), polythiophene (PTh), polypyrrole (PPy), polyfuran (PF), and polyaniline (PAn) with the structures given in the insets of Figs. 1 and 3 have quite interesting opti-

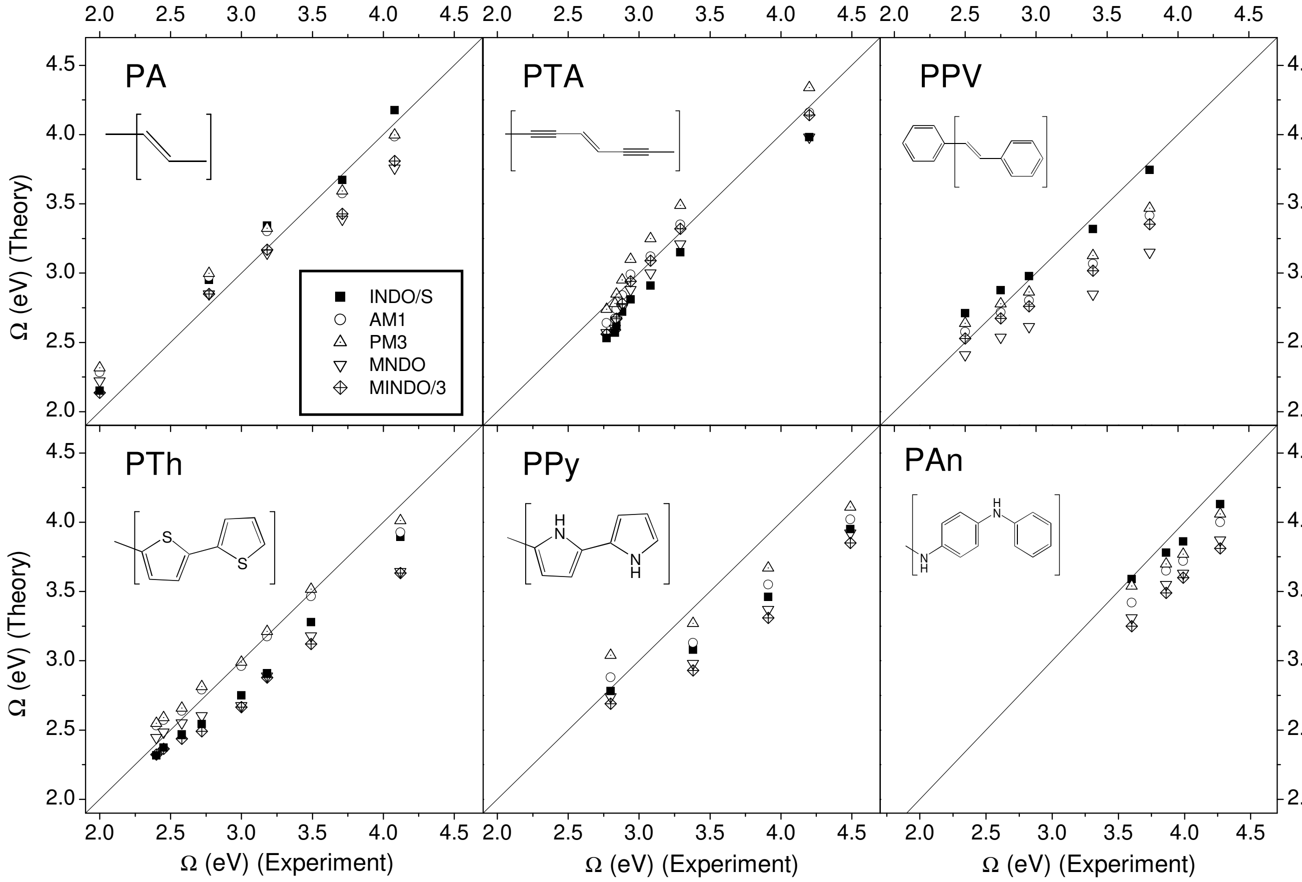

FIG. 1. Comparison of theoretical lowest transition energies (band-gap absorption maximum), computed with INDO/S, AM1, PM3, MNDO, and MINDO/3 Hamiltonians combined with CEO, with experimental data for conjugated oligomers with structures shown in the insets. Computations used the CEO code in the full active space. Exact agreement of theory and experiment gives points lying at the diagonal of the plots, whereas blue (red) shifted computed values vs. experimental data results in points lying higher (lower) than the diagonal.

cal properties and show promise in device applications [14–18,82–87]. We will compare results, obtained from different semiempirical parameterizations coupled with the CEO approach, with experiment tracking both absolute values and spectroscopic trends in absorption even though some deviations of theory from experiment are expected. Each conjugated oligomer of any polymer type has a strongly allowed low-lying singlet state of $1B_u$ symmetry showing up in linear absorption (band gap transition). In Fig. 1 we plot $1B_u$ transition frequencies of oligomers with various sizes computed for each semiempirical parameterization vs. experimental results reported in the literature for PA [88], PTA, [89] PPV [90], PTh [91,92], PPy [93–95], and PAn [96]. Each panel represents the oligomer shown in the inset, whereas groups of points correspond to the oligomers of different sizes. Points lying higher (lower) than the diagonal of the plot indicate that the computed value is blue (red) shifted compared to experiment. Excitation energies of different oligomers are well separated since band-gap transition energy shifts to the red with increasing chain length and gradually saturates to a constant for long chains [39,40]. This trend can be understood by analogy with the particle-in-a-box model. Fig. 1 suggests that overall the INDO/S results provide the best agreement with experiment. AM1 and PM3 values are very

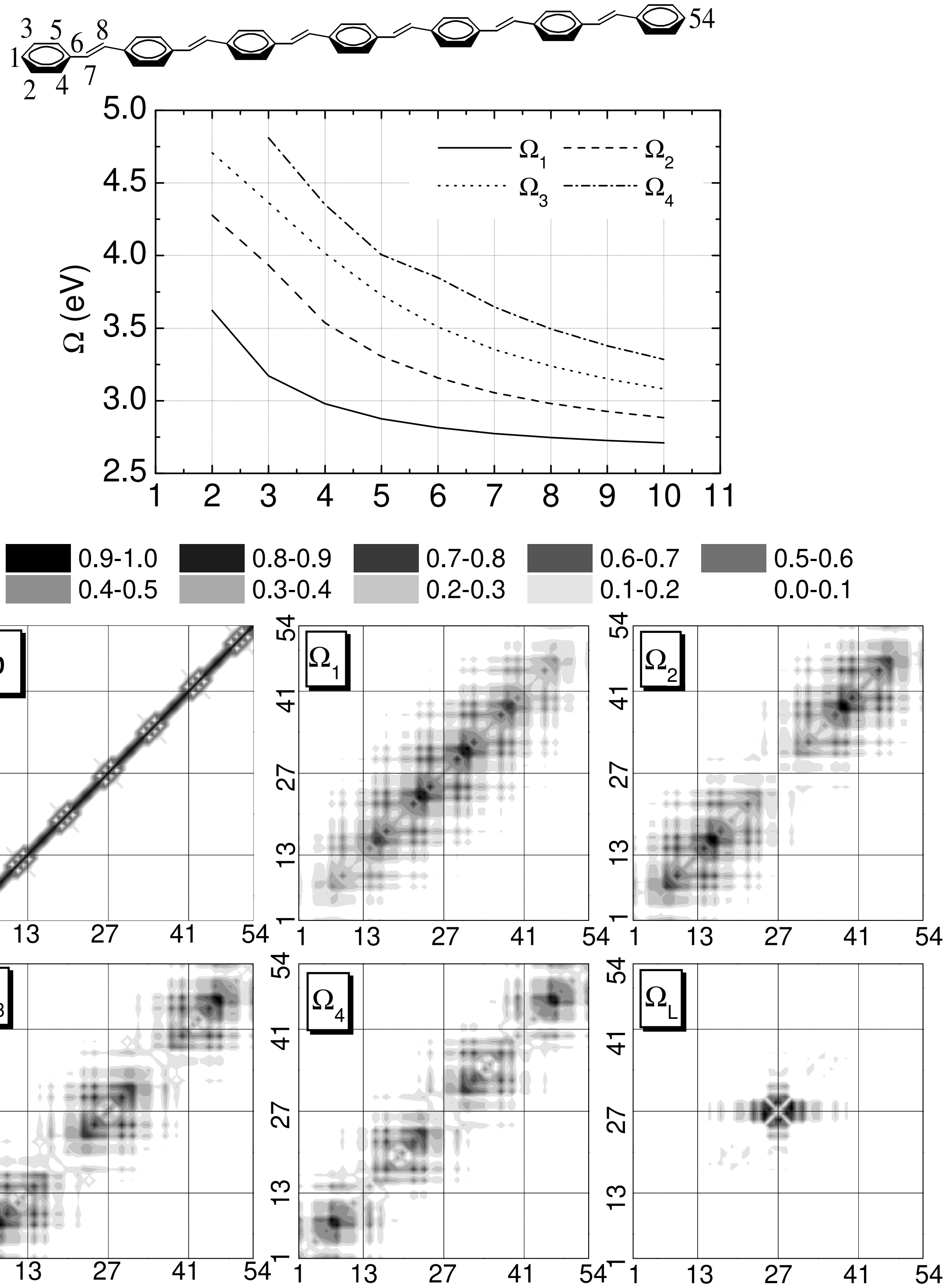

FIG. 2. Structure and atom labeling of PPV-7 oligomer (top). AM1 optimized planar structures have been used for CEO/INDO/S input. Computed variation of the four lowest excited state energies with the number of repeat units of the PPV chain (second row). Contour plots of the electronic modes of a PPV-7 monomer (bottom two rows). The axis labels represent the individual atoms and the tint map is given in the middle row goes from white (the smallest matrix elements) to black (the largest matrix elements). Panels ρ, $\Omega_1 - \Omega_4$, and Ω_L display the ground state density matrix and transition densities of the four lowest and localized transitions, respectively. The monomer mode frequencies $\Omega_1 - \Omega_4$ are 2.77, 3.05, 3.35, 3.64 eV, and $\Omega_L = 3.99$ eV. [39,40]

similar with small shift of PM3 energies to the blue. Compared with INDO/S, AM1 and PM3 results are shifted either to the blue (PTA, PTh, and PPy) or to the red (PA, PPV, PAn) and no universal trends could be discerned. MNDO and MINDO/3 give energies generally red-shifted compared to that of INDO/S.

We next analyze the electronic structure of PPV oligomers in detail. The top panel of Fig 2 shows the variation with oligomer size of energies corresponding to the four lowest electronic transitions. The energy of the lowest band-gap transition 1 (solid line), responsible for band gap transition, saturates to 2.7 eV for long chains, which compares well with the experimental value ~2.5 eV. The higher frequency transitions saturate at a slower rate going toward the lowest excitation saturated limit. All 4 excited states have B_u symmetry.

To trace the origin of the various peaks we have examined the corresponding collective electronic modes of a planar PPV-7 oligomer. Two-dimensional plots of the matrices ξ_ν [38,34,39,78,79] establish a direct link between the optical response and the underlying photoinduced real-space dynamics of charges. After contraction [40] the matrix size is equal to the number of carbon atoms, labeled according to Fig. 2. These matrices represent collective motions of electrons and holes and carry substantially less information than the complete many-electron eigenstates, but more than that required for calculating molecular polarizabilities and spectroscopic observables. The diagonal elements $(\xi_\nu)_{nn}$ represent the net charge induced on the n'th atomic orbital by an external optical field with frequency Ω_ν, whereas $(\xi_\nu)_{mn}$ $n \neq m$ is the dynamical bond-order (coherence) representing the joint amplitude of finding an electron on orbital m and a hole on orbital n [39].

To establish a reference point, panel ρ in Fig. 2 shows the ground state density matrix of PPV-7. This is diagonally localized, reflecting the nearest-neighbor chemical bonding in the ground state. Seven phenyl rings are clearly distinguishable. Panel Ω_1 shows the band-edge transition 1 and is very similar to that calculated with the PPP hamiltonian [39]. This picture shows that the electron-hole created upon optical excitation is delocalized over the whole chain (diagonal in the plot) and tends to be in the middle of the molecule. The exciton size (maximal distance between electron and hole) is about 4-5 repeat units (largest off-diagonal extent of the non-zero matrix area). Panel Ω_2 displays the next transition 2. This mode, forbidden in linear absorption, has the same off-diagonal coherence size as mode 1, but a non-uniform diagonal space distribution. The molecule is effectively broken into two parts with sizes of 3 repeat units and a very small electronic coherence between them. The electron-hole pair is located either in the first or in the second half of the chain, but not in the center. Two contributions to the transition dipole cancel each other resulting in a vanishing oscillator strength. The next transition 3 shown in panel Ω_3 is broken into the 3 parts. As shown in [34], the total contribution from the ends is approximately zero, and only the middle region contributes to the oscillator strength of this mode. This transition therefore makes only a weak contribution to the linear absorption. The molecule is effectively a trimer with weak electronic coherence among its parts. The off-diagonal coherence size is about 3 repeat units and the diagonal sizes are 2, 3, and 2 repeat units. The next mode (panel Ω_4) is broken into 4 parts and has a vanishing transition dipole since the contributions from the sub-quarters cancel each other. Finally the transitions in the higher frequency spectrum (3.5-7 eV) become localized to a single repeat unit and further to a single phenyl and a single vinyl groups [39]: For example the panel Ω_L electronic mode (forbidden in linear absorption) corresponds to the exciton localized on the central phenyl of the chain.

Thus the general trend of the electronic modes with increasing frequency is an effective aggregation of the molecule to small segments with weak electronic coherence among them.

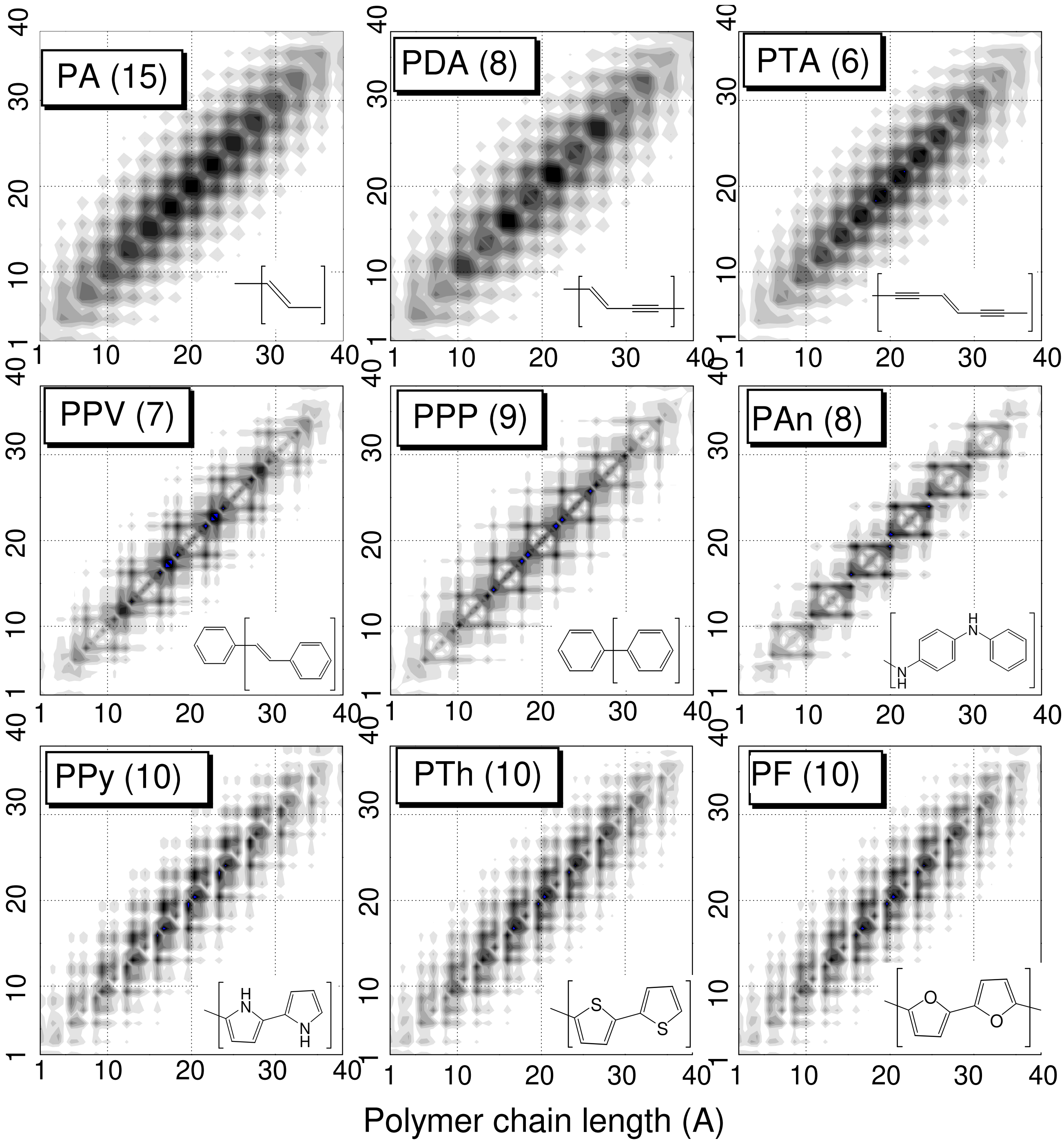

FIG. 3. Contour plots of the electronic modes computed with CEO/AM1 method corresponding to the band-gap transition in conjugated oligomers of approximately the same length (40 Å). Molecular structures are shown in the insets. The axis labels represent oligomer length in Å. The tint map is given in Fig. 2.

This is universal for larger polymers. The higher frequency modes tend to have more diagonal nodes [39,34,35]. The number of nodes is $n-1$, n being the mode number in the energy hierarchy (transition n in our notations). The mutual cancellation of the transition dipoles leads to vanishing oscillator strength of electronic modes with odd number of nodes, whereas the oscillator strength of electronic modes with even number of nodes scales as $\sim 1/n^2$. For example, the intensity of third transition with two nodes is about 9 times weaker than that of band gap $1B_u$ state. All electronic modes are almost symmetric with respect to the diagonal ($\xi_{mn} \approx \xi_{nm}$). This means that there is no preferred direction of motion for electrons (or holes). The electron-hole separation does not exceed 5 repeat units for all transitions, and the PPV-7 oligomer, therefore, well reflects the long chain limit.

We next examine the density matrices corresponding to band-gap transitions of different oligomers with similar chain length ($\sim$ 40 $\AA$). The transition densities are plotted in Fig. 3. The axes of each color panel show the coordinates of heavy atoms along the chain axis. All these plots are structurally similar: the electron-hole created upon optical excitation is delocalized over the whole chain (diagonal in the plot) and tends to be in the middle of the molecule. However, the exciton size (maximal distance between electron and hole) shown, as the largest off-diagonal extent of the non-zero matrix area, is different from polymer to polymer. PA, PDA, and PTA have the largest exciton size of about $\sim$ 20 $\AA$ (top row). This is reduced to $\sim$ 15 $\AA$ for PPV and PPP and to $\sim$ 10 $\AA$ for PAn (middle row). PPy, PTh, and PF, which have double bond conjugation paths similar to PA, again have large electron-hole delocalization of $\sim$ 20 $\AA$ (bottom row). In particular, large exciton size corresponds to the increased onset of band gap saturation for longer chains [21,39].

Finally we investigate how interchromophore interactions affect the electronic structure of molecules [40]. An important motivation for this study is related to designing technologically-relevant optoelectronic materials where the effect of aggregation is the major problem in achieving high luminescence quantum yields [97–102].

It is well understood that when the chromophores are well separated in space, their interaction is electrostatic (i.e. electron exchange or hopping is negligible). Each chromophore then retains its own electrons and the system may be described by a simple Frenkel exciton model common in molecular crystals and aggregated systems [103,104]. Each monomer peak splits into two transitions in the dimer spectra and their wavefunctions are symmetric and antisymmetric combinations of the monomeric excited states wavefunctions. This Davydov splitting [105–107] reflects interaction between chromophores and may be used to build an effective hamiltonian of the system [58,62,81]. However, the short-range electron exchange interaction becomes dominant when the distance between the chromophores is small. This strong interaction leads to charge transfer (CT) between molecules and formation of new localized electronic excitations. This general behavior has been understood for some time. In what follows, we will see the transition from Frenkel exciton to CT character occurs at an inter-oligomer distance of $\sim$4 $\AA$.

We use the 7 repeat unit (PPV-7) oligomer planar structure to create dimers consisting of two identical molecules which have phenyl-phenyl intersection (Fig. 4) at varying interchain separation $d = 3 - 10\AA$ with $0.1\AA$ step. Fig. 4 shows the variation of frequencies in dimer pair, corresponding to the band gap transition. Here, energies of Ω_1' and Ω_1'' are very close to the corresponding monomer energy Ω_1. Their splitting, as expected, increases with decreasing separation between chains, indicating a stronger interaction between monomer transition dipoles. These properties follow from the Frenkel exciton model for this simple aggregate.

To follow the evolution of the excited states at close intermolecular distances, we need to analyze the electronic modes in real-space which

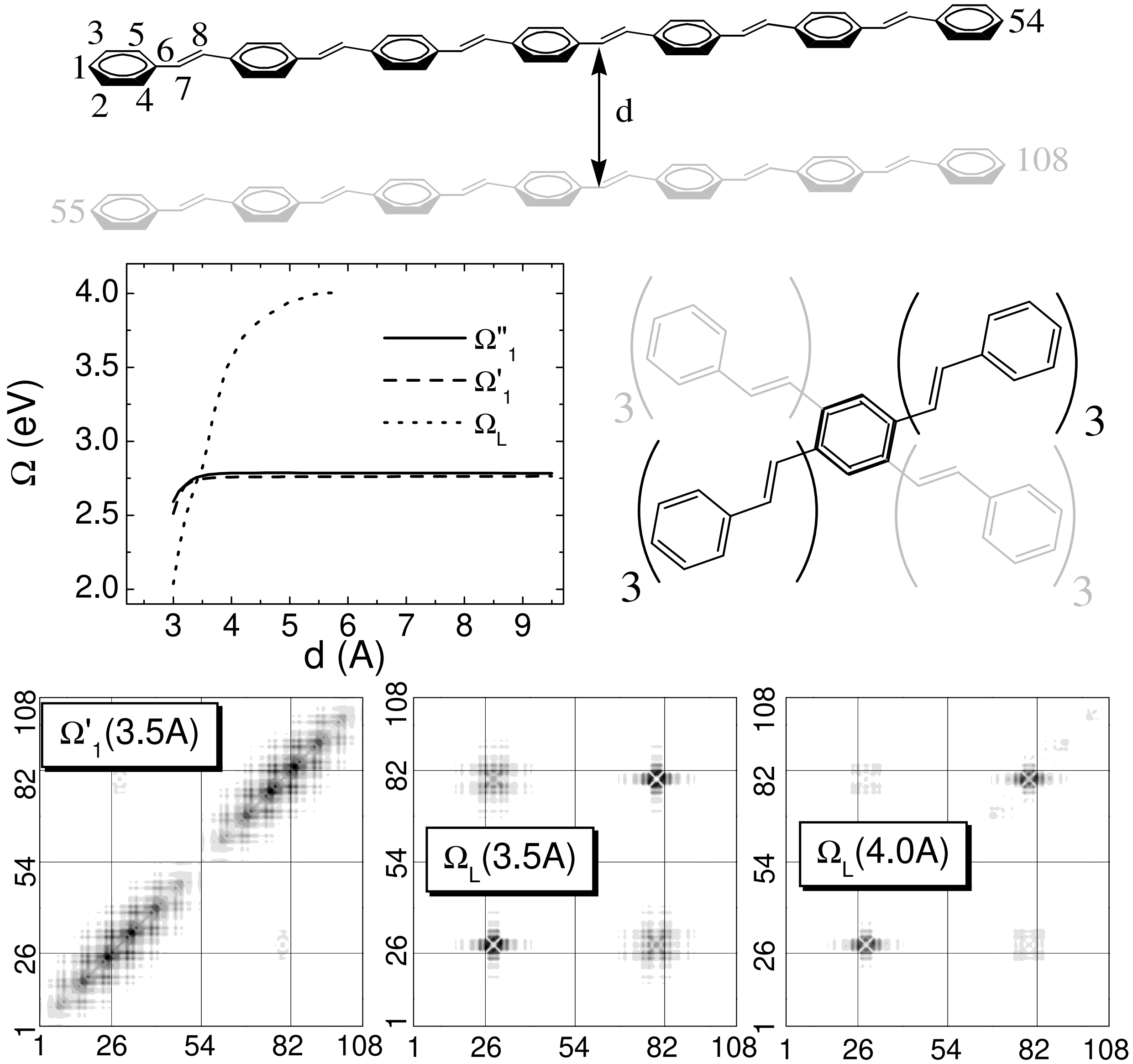

FIG. 4. Top: Structure and atom labeling of oligo-PPV dimer (side view). The interchain distance d has been varied (3-10 $\AA$) in CEO/INDO/S calculations. Intermolecular orientation is shown in case for phenyl-phenyl interaction (top view). Middle: Variation of excited state energies of delocalized (Ω_1', Ω_1'') and localized (Ω_L) transitions. Bottom: Contour plots of the relevant electronic modes of dimers at 3.5 and 4.0 $\AA$ separation. The axis labels represent the individual atoms, as shown in top panel. The tint map is given in the middle row of Fig. 2. [40]

provides a convenient method for identifying the electronic transitions. Atom labeling runs over monomer I first then over monomer II, following the top panel of Fig. 4. Even at close separations ($d = 3.5$ $\AA$) $1'$ (panel $\Omega_1'(3.5\mathrm{A})$ of Fig. 4) is simply the superposition of the monomeric 1 states (compare to Ω_1 in Fig. 2). The corners of the plot represent the monomers and there are only weak off-diagonal coherences between them which reflect coherent interaction between chromophores. The behavior of $1''$ electronic mode (not shown) is very similar to $1'$.

A prominent feature of the dimer spectrum is evolution of the L mode (panel Ω_L of Fig. 2) localized on the central phenyl. It is clear that L located at the contact should have the largest coherent interaction with its counterpart on the next molecule. Indeed, at $d = 4$ $\AA$ L (panel $\Omega_L(4.0\mathrm{A})$ of Fig. 4) already has noticeable coherence and its frequency is therefore red-shifted by 0.5 eV compared to Ω_L of monomer. Ω_L rapidly falls with decreasing intermolecular separation and it becomes the lowest mode in the electronic spectrum of dimer for $d \leq 3.5$ $\AA$ (Fig. 4). This red-shift is attributed to a significant intermolecular electron exchange and associated coherence (panel $\Omega_L(3.5\mathrm{A})$ of Fig. 4). Similar transitions localized on the two phenyls were computed with the CEO approach and observed experimentally in the spectra of the family of paracyclophane dimers [79,80]. Formation of such low-energy states in locations, where PPV-chain have close contacts (e.g. films), leads to effective fluorescence quenching [99–101]. Instead of emitting, excitons migrate to these low-energy traps which are non-emissive since L has a vanishing oscillator strength. It is interesting to notice that L does not mix with the 1 states even at 3.5 $\AA$ when L and $1''$ states are near-degenerate. This may be attributed to the nearly orthogonal nature of these states. These low-lying intermolecular states form for any contacts closer than ~ 4 $\AA$ [40] which may account for the reduced photoluminescence in these materials.

B. Size-scaling of nonlinear polarizabilities in donor/acceptor conjugated molecules.

Conjugated molecules usually possess large nonlinear polarizabilities due to their delocalized π-electron excitations [19,20,28,108]. Adding an electron-withdrawing and an electron-donating group enhances the nonlinear optical response even further [19,109–114]. These molecules have interesting optical properties which make them particularly promising materials for device applications. Understanding the mechanisms leading to dramatic changes in optical polarizabilities with increasing chain length and donor/acceptor strength, and the limiting factors of these enhancements are the key for a rational design strategy of molecules possessing large optical polarizabilities [115].

The variation of off-resonant optical polarizabilities of polyenes with molecular size may be described by the scaling law $\sim n^b$, n being the number of repeat units. In first (α) and third (γ) order responses the scaling exponents b vary considerably for short molecules: $1 < b_\alpha < 2$ and $2 < b_\gamma < 8$ [20,35,75,109,116–118]. For elongated chains, the exponent b attains the limiting value 1, indicating that the polarizabilities become extensive properties. Recent theoretical studies suggest that this sets in at about 30-50 repeat units. A saturation length was reported experimentally in one case [119] (corrected experimental value of ~ 60 repeat units have been published later in [120]). Establishing the precise scaling law of β and its the crossover to the bulk is the primary goal of experimental and theoretical studies. Experimental studies restricted by synthetic limitations to chain length of 11 repeat units show $1.4 < b_\beta < 3.2$ [19,110–113] whereas calculations performed with up to 22 repeat units yield $1.5 < b_\beta < 2$ [19,121].

The CEO technique provides a firm microscopic basis for predicting the size-scaling of molecular polarizabilities and pinpointing their origin. We start our investigation with quantitative comparison of calculated and experimen-

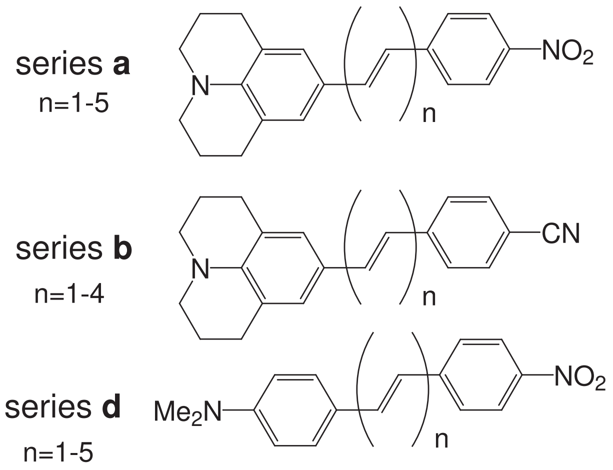

FIG. 5. Structures of push-pull donor/acceptor substituted diphenyl-polyene oligomers studied in [122].

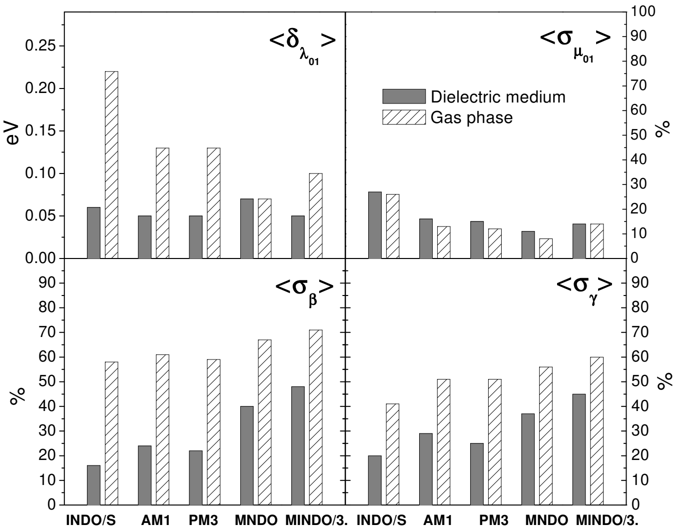

FIG. 6. Total averaged deviations of magnitudes of computed spectroscopic observables, for **a**, **b**, and **d** series in the dielectric medium and in the gas phase using model Hamiltonians, from the corresponding experimental values.

tal spectroscopic observables [123]. By combining the semiempirical Hamiltonians (INDO/S, AM1, PM3, MNDO, and MINDO/3) with the CEO approach we computed the lowest absorbing excited state (band-gap) energies and their transition dipoles, and the first (α), the second (β) and the third (γ) order static polarizabilities of several series of donor/acceptor substituted diphenyl-polyene oligomers with various sizes. These molecules are fairly small compared to limiting chain lengths when polarizabilities are expected to saturate [73–75]. Therefore, nonlinear polarizabilities of the considered substituted oligomers grow rapidly with increasing molecular size. Donor/acceptor compounds were synthesized and spectroscopically studied in [122]. In order to compare directly with experiment we have therefore used the Self Consistent Reaction Field (SCRF) approach, based on the Onsager model (Eq. (2.13)). In our computations, these substituted molecules have been treated (1) as isolated complexes (gas phase) with the dielectric constant $\epsilon = 1$, and (2) in a dielectric medium with $\epsilon = 2.219$ for the dioxane solvent used in experiment, and cavity radius a_0 computed with Gaussian package [27]. Fig. 6 shows the total deviation of computed values from the experimental results averaged over **a**, **b**, and **d** compounds. The computed excitation energies are reasonably accurate using any semiempirical model, and systematically improved when taking into account the solvent environment. Transition dipoles calculated with semiempirical Hamiltonians parameterized for the ground state (AM1, PM3, and MNDO) compare slightly more favorably with experiment than INDO/S values. The dielectric medium has very little effect on the transition dipole moments. Thus the simplest Onsager spherical cavity model, where an effective sphere radius is associated with the "real" molecular volume, performs fairly well in addressing the dielectric medium effects for the linear absorption spectrum.

The solvent environment has a dramatic effect on the magnitudes of nonlinear polarizabilities and has to be taken into account to reproduce experimental results. Polarizabilities computed with the INDO/S Hamiltonian parameterized for spectroscopic purposes show the best comparison with experimental results (on average 16% and 20% accuracy for the second and the third order static polarizabilities, respectively) [123]. In addition, the comparison with the ex-

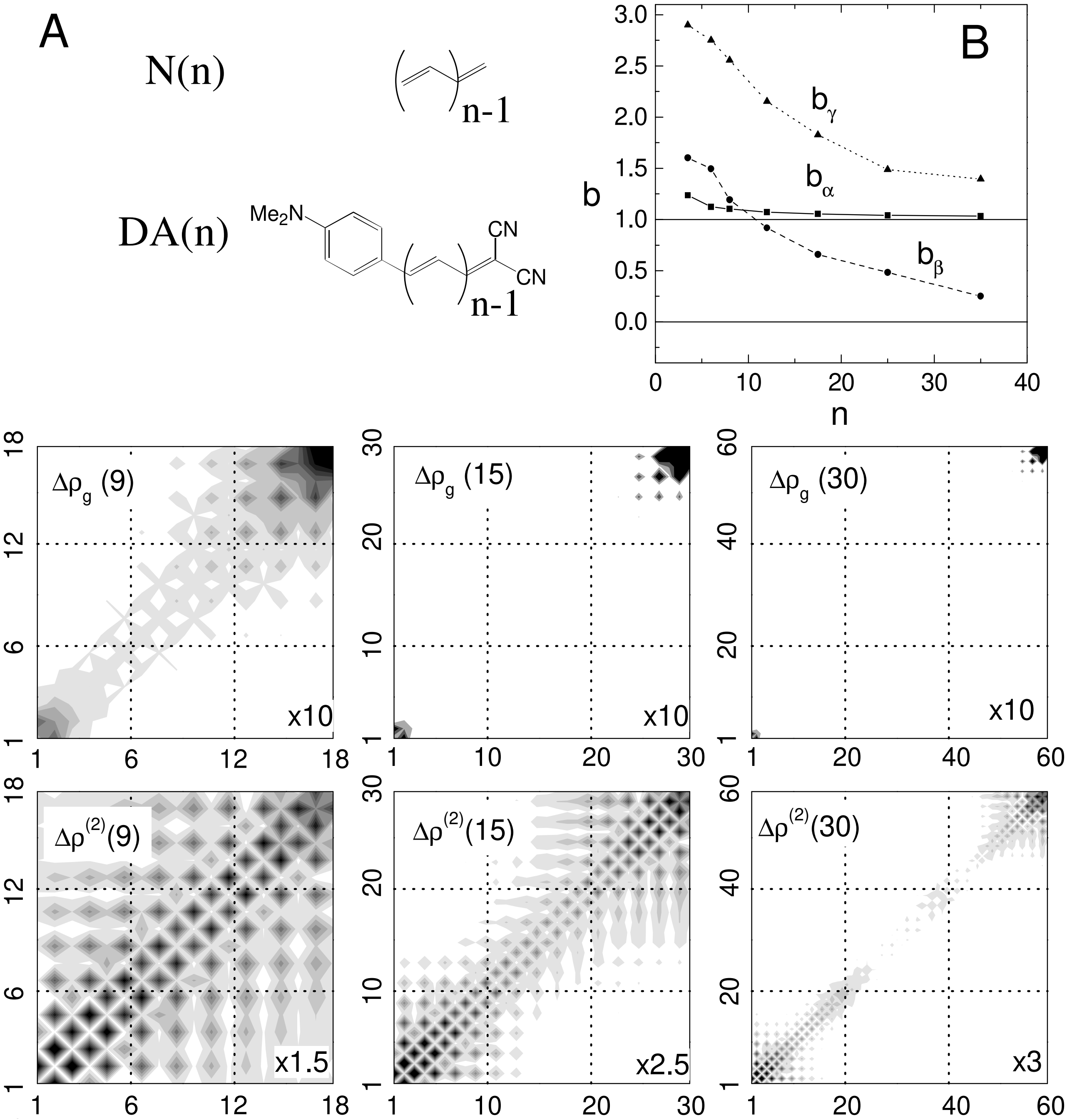

FIG. 7. A: Structures of the neutral $N(n)$ and Donor/Acceptor $DA(n)$ substituted molecules. Molecular geometries were optimized using AM1 model [30] in Gaussian 98 package [27]. Calculations were performed for bridges with n =5, 10, 15, 20, 30, 40 double bonds; B: Variation of the scaling exponents $b_\chi \equiv d[ln\chi]/d[lnn]$, $\chi = \alpha, \gamma, \delta$ with size for the these molecules. At large sizes b_α and b_γ tend to 1 whereas b_β approaches 0. These reflect the saturation of $\alpha/n, \gamma/n$, and β; Contour plots of the ground state difference matrices $\Delta\bar{\rho} = \bar{\rho}_{DA} - \bar{\rho}_N$ for n =9, 15, and 30 shown for the bridge part of the matrix. $\Delta\rho$ is magnified as indicated in each panel to use the same color code. Axes are labeled by the bridge carbon atoms with atom 1 on the donor side and atom $2n$ on the acceptor side. The second row displays the difference matrices to the second orders in the field $\Delta\rho^{(2)}$. The tint map is given in Fig. 2. [73,74]

periment for nonlinear polarizabilities of such large molecular systems is complicated because significant approximations (two- and three- level models or projection of the frequency dependent polarizability to the static limit) are usually invoked to estimate experimental values [122]. Nevertheless, the agreement with experiment for the series **a**, **b**, and **d** is encouraging. An additional caveat concerns the use of a more sophisticated solvent model to describe the dielectric medium effects. This investigation shows that a reasonably accurate computation of excitation energies, transition dipoles, and nonlinear static polarizabilities is possible by combining semiempirical parameterizations with the CEO technique for excited states. Careful choice of the optimal geometry and inclusion of dielectric medium effects significantly improve the quantitative comparison with the experimental data. The latter ingredient is extremely important for computing nonlinear polarizabilities which may be drastically enhanced by the solvent environment.

To study a size-scaling behavior of nonlinear polarizabilities we consider a family of unsubstituted (N(n)) and substituted with the donor and acceptor groups (DA(n)) molecules shown in Fig. 7(A). To disentangle the effects of donor-acceptor and bridge in the spectroscopy we study molecules with short (n=9), medium (n=15) and long (n=30) bridges. The calculated scaling exponents b_α, b_β and b_γ of donor/acceptor substituted polyenes are displayed in Fig. 7(B) [73]. As expected, b_α and b_γ reach the limiting value 1 at large sizes. b_β, however, is very different and vanishes at large sizes. This markedly different behavior of β can be explained by plotting the differences $\Delta\rho^{(2)} \equiv \delta\rho^{(2)}_{DA} - \delta\rho^{(2)}_{N}$ between the induced density matrices in the substituted and the neutral molecules (Fig. 7). This difference contributes to β. In complete analogy with the ground state where $\Delta\bar{\rho}$ (Fig. 7) defines μ_{gg} [73,74], the donor/acceptor influence is screened by the π electrons and is confined to a finite section of the bridge with about 15-17 double bonds. For short chains ($\Delta\rho^{(2)}(10)$) the donor and acceptor communicate directly since their influence regions overlap spatially; significant electronic coherence then develops between them. However, for larger chains $\Delta\rho^{(2)}(30)$ is block diagonal and their effects are clearly separable. This is the reason why β levels off to a constant with $b_\beta = 0$: only the ends of the molecule contribute to β whereas the middle part is identical to that of neutral molecule and only contributes to α and γ [45].

Defining and predicting the saturation size of optical properties is a key factor in developing synthetic strategies for optical materials. The two-dimensional CEO plots provide a highly intuitive yet quantitative tool for addressing this problem: the density matrix shows that the influence of the donor or the acceptor is limited to a few double bonds in its vicinity; the size of these coherence regions depends on the donor and the acceptor strength. Direct donor-to acceptor charge transfer does occur at short chains. However when the molecular size is larger than the coherence size the donor and the acceptor are decoupled and their effects are additive; β itself (rather than β/n) then become size-independent.

IV. DISCUSSION

The connection between electronic structure and optical properties of organic compounds constitutes a complex fundamental problem with important technological implications. There is a clear need for computational methods which provide intuitive and compact interpretation of obtained results. In addition, calculated spectroscopic observables should be reliable and quantitatively reproduce experimental data for wide variety of molecular systems. Described in this review CEO approach offers such capabilities. This method combines different semiempirical Hamiltonians (INDO/S [42,50], AM1 [30], PM3 [31], MNDO [32], MINDO/3 [33]) with the RPA approximation for the many-electron wavefunction [37]. It has several computational advantages: instead of arbitrary truncation of molecular orbitals, the fast Krylov space algorithms (Lanczos, Davidson, and IDSMA) take into account all molecular orbital space included in the TDHF approximation, making such calculations straightforward to apply. Yet, the computational cost per excited state is very low and usually does not exceed that of the ground state. This makes excited state structure calculations possible whenever SCF ground state computations are available.

Numerical comparison of computed results where possible against existing experimental data shows that spectroscopic observables agree well with experiment. The INDO/S semiempirical parameterization show the best agreement because INDO/S was primarily designed for this purpose. However, this approximation is not adequate for the ground state. On the other hand, AM1, PM3, and MNDO results show reasonable agreement with experiment and reproduce the basic trends. Also, these semiempirical Hamiltonians are more reliable for molecular ground state properties at the Hartree-Fock level since they were parameterized for this purpose. The computed excitation energies are very accurate using any semiempirical model, and systematically improved when taking into account the solvent environment. Transition dipoles calculated with semiempirical Hamiltonians parameterized for the ground state (AM1, PM3, and MNDO) compare slightly more favorably with experiment than INDO/S values. The dielectric medium has very little effect on the transition dipole moments. Thus the simplest Onsager spherical cavity model, where an effective sphere radius is associated with the "real" molecular volume, performs fairly well in addressing the dielectric medium effects for the linear absorption spectrum. The solvent environment has a dramatic effect on the magnitudes of nonlinear polarizabilities and has to be taken into account to reproduce experimental results. Polarizabilities computed with the INDO/S Hamiltonian parameterized for spectroscopic purposes show the best comparison with experimental results (on average 16% and 20% accuracy for the second and the third order static polarizabilities, respectively).

The CEO density matrix approach carries less information but at considerably lower cost, making it readily applicable to the interesting crossover region between small molecules and bulk. The electronic density matrix associated with nonlinear optical response may be easily obtained by summing over the electronic oscillators coupled by relevant nonlinear dipole. Limiting interference effects resulting in the SOS approach in an almost complete cancellation of large contributions to optical susceptibilities [116,117,124,125], are built-in in the CEO method from the start and each separate contribution to the susceptibility scales properly [37]. In addition, the CEO results allow the analysis of optical spectra in terms of charge distributions in excited states and motions of electrons and holes in real space. The two-dimensional real-space analysis of the relative motion of electron-hole pairs proved to be very useful in the interpretation of optical properties in both conjugated molecules [34,35,39,73,126] and molecular aggregates [38,40,58,78,79,126]. A new type of chemical intuition which focuses directly on the electronic charges and coherences and is not based on properties of many-electron eigenstates emerges naturally: In addition to the charge density [127], the coherences make it possible to directly view how different parts of the molecule are coupled and how a perturbation at one point can affect the electronic motion at other regions.

We conclude that an accurate computation of excitation energies, transition dipoles, and nonlinear static polarizabilities is possible by combining INDO/S, AM1, PM3, or MNDO semiempirical parameterizations with the CEO technique for excited states. Careful choice of the optimal geometry and inclusion of dielectric medium effects significantly improve the quantitative comparison with the experimental data. The latter ingredient is extremely important for computing nonlinear polarizabilities which may be drastically enhanced by the solvent environment. The CEO method maps optical spectra directly to the motions of electrons and holes in real space by generating the optically-driven reduced single electron density matrix. This makes possible two-dimensional real-space analysis of relative motion of electron-hole pairs for any electronic transition. In turn, this is very useful for the interpretation of optical properties in conjugated molecules and constitutes an important advantage of the theoretical approach when combined with any semiempirical Hamiltonian.

V. ACKNOWLEDGEMENTS

This research is supported by the US Department of Energy and the LDRD program at LANL.

---

[1] J. Burroughes, D. D. C. Bradley, A. Brown, R. Marks, K. Mackay, R. H. Friend, P. Burns, and A. Holmes, *Nature* **347**, 539 (1990).

[2] D. Braun and A. J. Heeger, *Appl. Phys. Lett.* **58**, 1982 (1991).

[3] Q. B. Pei, G. Yu, C. Zhang, Y. Yang, and A. J. Heeger, *Science* **269**, 1086 (1995).

[4] G. Yu, J. Gao, J. C. Hummelen, F. Wudl, and A. J. Heeger, *Science* **270**, 1789 (1995).

[5] H. Sirringhaus, N. Tessler, and R. H. Friend, *Science* **280**, 1741 (1998).

[6] P. K. H. Ho, D. S. Thomas, R. H. Friend, and N. Tessler, *Science* **285**, 233 (1999).

[7] A. Dodabalapur, Z. Bao, A. Makhja, J. C. Laquindanum, V. R. Raju, Y. Feng, H. E. Katz, and J. Rogers, *Appl. Phys. Lett.* **73**, 142 (1998).

[8] G. Yu, K. Pakbaz, and A. J. Heeger, *Appl. Phys. Lett.* **64**, 3422 (1994).

[9] H. Yu, B. R. Hsieh, M. A. Abkowitz, S. A. Jenekhe, and M. Stolka, *Synthetic Metals* **62**, 265 (1994).

[10] H. E. Katz, *J. Mater. Chem.* **7**, 369 (1997).

[11] D. J. Gundlach, Y. Y. Lin, T. N. Jackson, and D. G. Schlom, *Appl. Phys. Lett.* **71**, 3953 (1997).

[12] F. Hide, M. A. D. Garsia, B. J. Schwartz, M. R. Andersson, Q. B. Pei, and A. J. Heeger, *Science* **273**, 1833 (1996).

[13] N. Tessler, G. J. Denton, and R. H. Friend, *Nature* **382**, 695 (1996).

[14] S. V. Frolov, W. Gellerman, M. Ozaki, K. Yoshino, and Z. V. Vardeny, *Phys. Rev. Lett.* **78**, 729 (1997).

[15] J. H. Schon, A. Dodabalapur, C. Kloc, and B. Batlogg, *Science* **289**, 299 (2000).

[16] J. H. Schon, A. Dodabalapur, C. Kloc, and B. Batlogg, *Science* **290**, 963 (2000).

[17] J. H. Schon, C. Kloc, H. Y. Hwang, and B. Batlogg, *Science* **292**, 251 (2001).

[18] R. Pachter, R. Crane, and W. W. Adams, *Materials Research Society Symposia Proceedings* **374**, 39 (1995).

[19] D. R. Kanis, M. A. Ratner, and T. J. Marks, *Chem. Rev.* **94**, 195 (1994).

[20] J. L. Brédas, C. Adant, P. Tackyx, A. Persoons, and B. M. Pierce, *Chem. Rev.* **94**, 243 (1994).

[21] J. L. Brédas, J. Cornil, D. Beljonne, D. A. D. Santos, , and Z. Shuai, *Acc. Chem. Res.* **32**, 267 (1999).

[22] A. Szabo and N. S. Ostlund, *Modern Quantum Chemistry: Introduction to Advanced Electronic Structure Theory* (McGraw-Hill, New York, 1989).

[23] F. S. Spano and Z. G. Soos, *J. Chem. Phys.* **99**, 9265 (1993).

[24] E. R. Stratmann, G. E. Scuseria, and M. J. Frisch, *J. Chem. Phys.* **109**, 8218 (1998).

[25] R. Bauernschmitt, R. Ahlrichs, F. H. Hennrich, and M. M. Kappes, *J. Am. Chem. Soc.* **120**, 5052 (1998).

[26] M. E. Casida, in *Recent Advances in Density-Functional Methods*, Vol. 3 of *Part I*, edited by D. A. Chong (World Scientific, Singapore,

1995).

[27] M. J. Frisch *et al.*, *Gaussian 98 (Revision A.9)* (Gaussian, Inc., Pittsburgh PA, 1999).

[28] *Nonlinear Optical Properties of Organic Molecules and Crystals*, edited by J. Zyss and D. S. Chemla (Academic Press, Florida, 1987), Vol. 1 and 2.

[29] J. A. Pople, D. L. Beveridge, and P. Dobosh, *J. Chem. Phys.* **47**, 2026 (1967).

[30] M. J. S. Dewar, E. G. Zoebisch, E. F. Healy, and J. J. P. Stewart, *J. Am. Chem. Soc.* **107**, 3902 (1985).

[31] J. J. P. Stewart, *J. Comp. Chem.* **10**, 210 (1989).

[32] M. J. S. Dewar and W. Thiel, *J. Am. Chem. Soc.* **99**, 4899 (1977).

[33] M. J. S. Dewar, R. C. Bingham, and D. H. Lo, *J. Am. Chem. Soc.* **97**, 1285 (1975).

[34] S. Tretiak, V. Chernyak, and S. Mukamel, *J. Am. Chem. Soc.* **119**, 11408 (1997).

[35] S. Tretiak, V. Chernyak, and S. Mukamel, *Chem. Phys. Lett.* **259**, 55 (1996).

[36] P. Ring and P. Schuck, *The Nuclear Many-Body Problem* (Springer-Verlag, New York, 1980).

[37] V. Chernyak and S. Mukamel, *J. Chem. Phys.* **104**, 444 (1996).

[38] S. Tretiak, V. Chernyak, and S. Mukamel, *J. Phys. Chem. B* **102**, 3310 (1998).

[39] S. Mukamel, S. Tretiak, T. Wagersreiter, and V. Chernyak, *Science* **277**, 781 (1997).

[40] S. Tretiak, A. Saxena, R. L. Martin, and A. R. Bishop, *J. Phys. Chem. B* **104**, 7029 (2000).

[41] V. Chernyak, S. Tretiak, M. Schulz, E. V. Tsiper, and S. Mukamel, *J. Chem. Phys.* **113**, 36 (2000).

[42] J. Ridley and M. C. Zerner, *Theor. Chim. Acta* **32**, 111 (1973).

[43] J. E. Ridley and M. C. Zerner, *Theoret. Chim. Acta* **42**, 223 (1976).

[44] J. J. P. Stewart, *MOPAC manual* (Schrödinger Inc. and Fujitsu Limited, Portland, OR 97201, 2000).

[45] S. Tretiak, V. Chernyak, and S. Mukamel, *J. Chem. Phys.* **105**, 8914 (1996).

[46] E. V. Tsiper, *JETP Letters* **70**, 751 (1999).

[47] E. V. Tsiper, unpublished, preprint cond-mat/0003164 @ xxx.lanl.gov, 2000.

[48] E. R. Davidson, *J. Comput. Phys.* **17**, 87 (1975).

[49] M. C. Zerner, *A General Semiempirical Program Package, ZINDO* (Department of Biochemistry, University of Florida, Gainesville, FL, 1998).

[50] M. C. Zerner, G. H. Loew, R. F. Kirchner, and U. T. Mueller-Westerhoff, *J. Am. Chem. Soc.* **102**, 589 (1980).

[51] A. D. Bacon and M. C. Zerner, *Theoret. Chim. Acta* **53**, 21 (1979).

[52] E. V. Tsiper, V. Chernyak, S. Tretiak, and S. Mukamel, *Chem. Phys. Lett.* **302**, 77 (1999).

[53] E. V. Tsiper, V. Chernyak, S. Tretiak, T. Meier, and S. Mukamel, *J. Chem. Phys.* **110**, 8328 (1999).

[54] M. Tommasini, V. Chernyak, and S. Mukamel, *J. Phys. Chem.* (in press) (2001).

[55] M. G. Cory, M. C. Zerner, X. Hu, and X. K. Schulten, *J. Phys. Chem.* **102**, 7640 (1998).

[56] G. Karlsson and M. C. Zerner, *Int. J. Quantum Chem.* **7**, 35 (1973).

[57] G. Karlsson and M. C. Zerner, *J. Phys. Chem.* **96**, 6949 (1992).

[58] S. Tretiak, C. Middleton, V. Chernyak, and S. Mukamel, *J. Phys. Chem. B* **104**, 4519 (2000).

[59] E. E. Moore and D. Yaron, *J. Chem. Phys.* **109**, 6147 (1998).

[60] E. E. Moore, B. F. Gherman, and D. Yaron, *J. Chem. Phys.* **106**, 4216 (1997).

[61] R. Cammi, B. Mennucci, and J. Tomasi, *J. Phys. Chem. A* **102**, 870 (1998).

[62] S. Tretiak, C. Middleton, V. Chernyak, and S. Mukamel, *J. Phys. Chem. B* **104**, 9540 (2000).

[63] E. R. Davidson, *Reduced Density Matrices in Quantum Chemistry* (Academic Press, New York, 1976).

[64] R. McWeeny and B. T. Sutcliffe, *Methods of Molecular Quantum Mechanics* (Academic Press, New York, 1976).

[65] A. Takahashi and S. Mukamel, *J. Chem. Phys.* **100**, 2366 (1994).

[66] M. Hartmann, V. Chernyak, and S. Mukamel, *Phys. Rev. B* **52**, 2528 (1995).

[67] S. Rettrup, *J. Comp. Phys.* **45**, 100 (1982).

[68] K. B. Wiberg, E. R. Stratmann, and M. J. Frisch, *Chem. Phys. Lett.* **297**, 60 (1998).

[69] Y. Saad, *Numerical Methods for Large Eigenvalue Problems* (Manchester, University Press, 1992).

[70] B. N. Parlett, *Symmetric Eigenvalue Problem* (Prentice Hall, Englewood Cliffs, 1980).

[71] H. Weiss, R. Ahlrichs, and M. Häser, *J. Chem Phys.* **99**, 1262 (1993).

[72] J. Olsen, H. Jorden, A. A. Jensen, and P. Jorgensen, *J. Comput. Phys.* **74**, 265 (1988).

[73] S. Tretiak, V. Chernyak, and S. Mukamel, *Chem. Phys. Lett.* **287**, 75 (1998).

[74] S. Tretiak, V. Chernyak, and S. Mukamel, *Chem. Phys.* **245**, 145 (1999).

[75] S. Tretiak, V. Chernyak, and S. Mukamel, *Phys. Rev. Lett.* **77**, 4656 (1996).

[76] S. Tretiak, V. Chernyak, and S. Mukamel, *Chem. Phys. Lett.* **297**, 357 (1998).

[77] S. Tretiak, C. Middleton, V. Chernyak, and S. Mukamel, in *Photoinduced Charge Transfer*, edited by L. Rothberg (World Scientific, New Jersey, 2000).

[78] S. Tretiak, W. M. Zhang, V. Chernyak, and S. Mukamel, *Proc. Nat. Acad. Sci. USA* **96**, 13003 (1999).

[79] G. C. Bazan, W. J. Oldham, R. J. Lachicotte, S. Tretiak, V. Chernyak, and S. Mukamel, *J. Am. Chem. Soc.* **120**, 9188 (1998).

[80] S. Wang, G. C. Bazan, S. Tretiak, and S. Mukamel, *J. Am. Chem. Soc.* **122**, 1289 (2000).

[81] E. Poliakov, V. Chernyak, S. Tretiak, and S. Mukamel, *J. Chem. Phys.* **110**, 8161 (1999).

[82] G. Gustafson, Y. Gao, G. M. Treacy, F. Klauetter, N. Colaneri, and A. Heeger, *Nature* **357**, 477 (1992).

[83] N. C. Greenham, S. C. Maratti, D. D. C. Bradley, A. B. Holmes, and R. H. Friend, *Nature* **65**, 628 (1993).

[84] N. Tessler, D. J. Denton, and R. H. Friend, *Nature* **382**, 695 (1996).

[85] D. D. C. Bradley, *Nature* **382**, 671 (1996).

[86] Proceedings of the International Conference on Synthetic Metals ICSM 96, *Synthetic Metals*, **84**, 1997.

[87] M. A. Baldo, M. E. Thompson, and S. R. Forrest, *Nature* **403**, 750 (2000).

[88] F. Sondheimer, D. A. Ben-Efraim, and R. Wolovsky, *J. Am. Chem. Soc.* **83**, 1675 (1961).

[89] U. Gubler, C. Bosshard, P. Günter, M. Y. Balakina, J. Cornil, J. L. Brédas, R. E. Martin, and F. Diederich, *Opt. Lett.* **24**, 1599 (1999).

[90] J. Cornil, D. Beljonne, C. M. Heller, I. H. Campbell, B. K. Laurich, D. L. Smith, D. D. C. Bradley, K. Mullen, and J. L. Brédas, *Chem. Phys. Lett.* **278**, 139 (1997).

[91] H. Chosrovian, S. Rentsch, D. Grebner, D. U. Dahm, and E. Birckner, *Synth. Met.* **60**, 23 (1993).

[92] R. A. J. Janssen, N. S. S. L. Smilowitz and, and D. Moses, *J. Chem. Phys.* **101**, 1787 (1994).

[93] W. C. Price and A. D. Wallsh, *Proc. R. Soc. London* **179A**, 20 (1941).

[94] W. M. Flicker, O. A. Mosher, and A. Kuppermann, *J. Chem. Phys.* **64**, 1315 (1976).

[95] J. M. Ribó, M. C. Anglada, J. M. Tura, and N. Ferrer-Anglada, *Synth. Met.* **72**, 73 (1995).

[96] M. I. Boyer, S. Quillard, G. Louarn, and S. Lefrant, *Synth. Met.* **101**, 782 (1999).

[97] S. A. Jenekhe and J. A. Osaheni, *Science* **265**, 765 (1994).

[98] E. Conwell, *Trends in Polym. Sci.* **5**, 218 (1997).

[99] R. Jakubiak, C. J. Collison, B. R. H. W. Chou Wan and, and L. J. Rothberg, *J. Phys. Chem.* **103**, 2394 (1999).

[100] M. Yan, L. J. Rothberg, F. Papadimitrakopoulos, M. E. Galvin, and T. Miller, *Phys. Rev. Lett.* **73**, 744 (1994).

[101] M. Yan, L. J. Rothberg, E. W. Kwock, and T. M. Miller, *Phys. Rev. Lett.* **75**, 1992 (1975).

[102] D. W. McBranch and M. B. Sinclair, in *The Nature of the Photoexcitations in Conjugated Polymers*, edited by N. S. Sariciftci (Word Scientific Publishing, Singapore, 1997).

[103] M. Pope and C. E. Swenberg, *Electronic Pro-*

cesses in Organic Crystals (Clarendon Press, Oxford University Press, Oxford, New York, 1982).

[104] E. A. Silinsh and V. Čápek, *Organic Molecular Crystals* (AIP Press, American Institute of Physics, New York, 1994).

[105] M. Kasha, H. R. Rawls, and M. A. El-Bayoumi, *Pure and Applied Chem.* **11**, 371 (1965).

[106] E. I. Rashba and M. D. Sturge, *Excitons* (North-Holland, Amsterdam, 1982).

[107] V. B. Broude, E. I. Rashba, and E. F. Sheka, *Spectroscopy of Molecular Excitons* (Springer, Berlin, 1985).

[108] T. Toury, J. Zyss, V. Chernyak, and S. Mukamel, *J. Chem. Phys.* (Submitted) (2000).

[109] C. Bubeck, Nonlinear Optical Material: Principles and Applications, edited by V. Degiorgio and C. Flytzanis (IOS Press, Amsterdam 1995), p.359.

[110] M. Blanchard-Desce, C. Runser, A. Fort, M. Barzoukas, J.-M. Lehn, V. Bloy, and V. Alain, *Chem. Phys.* **199**, 253 (1995).

[111] M. Blanchard-Desce, J.-M. Lehn, M. Barzoukas, I. Ledoux, and J. Zyss, *Chem. Phys.* **181**, 281 (1994).

[112] M. Blanchard-Desce, J.-M. Lehn, M. Barzoukas, C. Runser, A. Fort, G. Puccetti, I. Ledoux, and J. Zyss, *Nonlinear Optics* **10**, 23 (1995).

[113] M. Blanchard-Desce, R. Woltmann, S. L. J.-M. Lehn, and P. Kramer, *Chem. Phys. Lett.* **243**, 526 (1995).

[114] J. O. Morley, *J. Chem. Soc. Perkins Trans.* **II**, 1351 (1987).

[115] S. R. Marder, B. Kippelen, A. K.-Y. Jen, and N. Peyghambarian, *Nature* **388**, 845 (1997).

[116] J. F. Heflin, K. Y. Wong, Q. Zamani-Khamini, and A. F. Garito, *Phys. Rev. B* **38**, 1573 (1988).

[117] D. C. Rodenberger, J. F. Heflin, and A. F. Garito, *Nature* **359**, 309 (1992).

[118] C. Flytzanis and J. Huttler, in *Contemporary Nonlinear Optics*, edited by G. P. Agrawal and R. W. Boyd (Academic Press, San Diego, 1992).

[119] I. D. W. Samuel, I. Ledoux, C. Dhenaut, J. Zyss, H. H. Fox, R. R. Schrock, and R. J. Silbey, *Science* **265**, 1070 (1994).

[120] I. Ledoux, I. D. W. Samuel, J. Zyss, S. N. Yaliraki, F. J. Schattenmann, R. R. Schrock, and R. J. Silbey, *Chem. Phys.* **245**, 1 (1999).

[121] N. Matsuzawa and D. A. Dixon, *Int. J. Quantum Chemistry* **44**, 497 (1992).

[122] V. Alain, S. Rédoglia, M. Blanchard-Desce, S. Lebus, K. Lukaszuk, R. Wortmann, U. Gubler, C. Bosshard, and P. Günter, *Chem. Phys.* **245**, 51 (1999).

[123] S. Tretiak, A. Saxena, R. L. Martin, and A. R. Bishop, *J. Chem. Phys.* (in press) (2001).

[124] S. Mukamel, *Principles of Nonlinear Optical Spectroscopy* (Oxford, New York, 1995).

[125] D. Yaron, *Phys. Rev. B* **54**, 4609 (1996).

[126] S. Tretiak, Ph.D. thesis, University of Rochester, Rochester, NY, 1998.

[127] R. F. W. Bader, *Atoms in molecules: a quantum theory* (Oxford, New York: Clarendon Press, 1990).